Tuning the Surface Reactivity and Tribological Performance of Phosphonium-Based Ionic Liquid at Steel/Steel Interfaces by Bromide/Phosphate Anion Mixtures

Zixuan Li,^{1,2} Hugo Celio,¹ Andrei Dolocan,¹ Nicolás Molina,^{1,2} Jude Kershaw,³ Oscar Morales-Collazo,³ Joan F. Brennecke,³ Filippo Mangolini^{1,4*}

- 1. Texas Materials Institute, The University of Texas at Austin, Austin, Texas 78712, USA
- Materials Science and Engineering Program, The University of Texas at Austin, Austin, Texas 78712, USA
 - 3. McKetta Department of Chemical Engineering, The University of Texas at Austin, Austin, Texas 78712, USA
- 4. Walker Department of Mechanical Engineering, The University of Texas at Austin, Austin, Texas 78712, USA

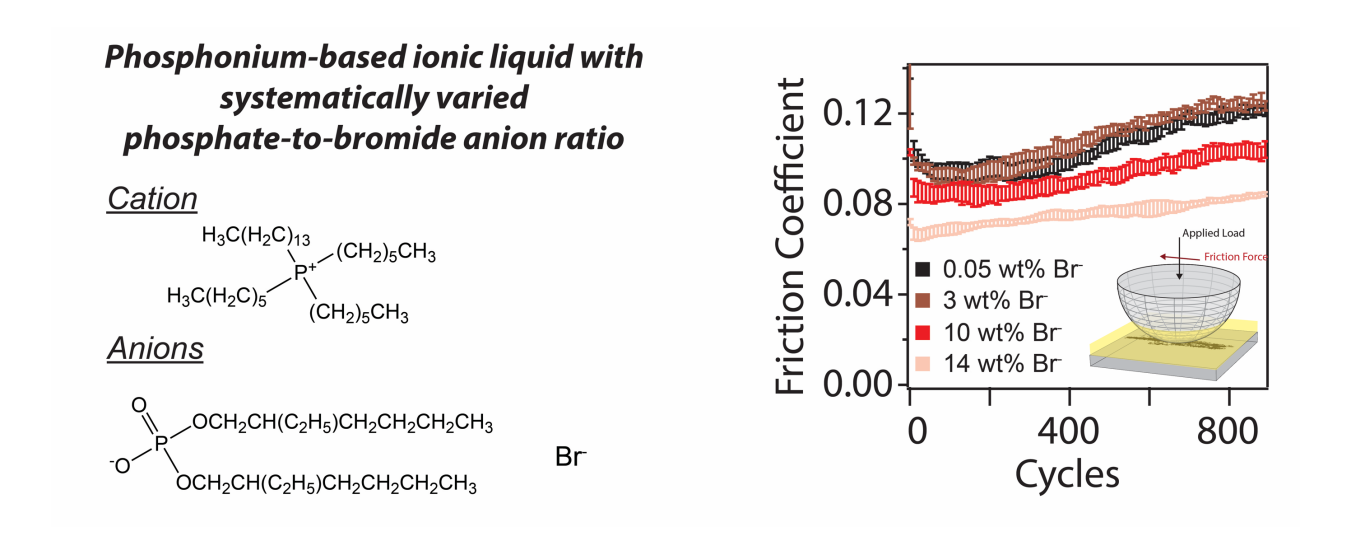
filippo.mangolini@austin.utexas.edu

^{*} Author to whom correspondence should be addressed. Email:

ABSTRACT

Phosphonium phosphate ionic liquids (ILs) are promising lubricant additives for engine oils owing to a combination of good tribological performance and attractive properties, such as high thermal stability and good miscibility with mineral and synthetic oils. Here, we evaluate the dependence of the lubricating performance of trihexyltetradecylphosphonium ([P_{6,6,6,14}])-based ILs when used in steel/steel contacts on the relative concentration of bis(2-ethylhexylphosphate ([DEHP]) and bromide (Br') anions. The results indicate no changes in friction and wear upon increasing the [P_{6,6,6,14}]Br-to-[P_{6,6,6,14}][DEHP] volume ratio up to 0.2:1, while a further increase in this ratio leads to a reduction of friction and wear. X-ray photoelectron spectroscopy and time-of-flight secondary ion mass spectrometry measurements highlight that the dependence of the lubricating properties of the ILs on the [P_{6,6,6,14}]Br-to-[P_{6,6,6,14}][DEHP] ratio originates from the balance between corrosivity and surface reactivity of this IL: while [DEHP] acts as corrosion inhibitor in the non-contact region, the formation of species containing phosphorus-oxygen moieties in the wear track as a result of the hydrolysis of phosphonium ions increases the surface coverage of phosphorus. This is proposed to decrease friction by decreasing adhesion at steel/steel contacts and lowering the interfacial shear strength.

GRAPHICAL ABSTRACT



KEYWORDS Ionic liquid; phosphonium phosphate; lubrication; corrosion; halides

1. INTRODUCTION

Ionic liquids (ILs) have been extensively studied in the last two decades as potential environmentally friendly boundary lubricants owing to their promising tribological performance [1–3], and their intrinsic properties such as high thermal stability, low flammability, and low vapor pressure [4,5]. At the molecular level, ILs are known to have distinctive behaviors upon nanoconfinement [6]. The spatial confinement of ILs in nanoscale geometries, which has usually been assessed by surface force apparatus (SFA) and colloidal atomic force microscopy (AFM) experiments, can not only result in significant variations in physical properties of ILs compared to the ones of bulk ILs, but also promote their interaction with the confining solids and the formation of an ordered, layered structure, which exhibits a high resistance to being squeezed out. This unique behavior of ILs under nanoscale confinement has been proposed to be the origin of their ability to reduce friction and protect sliding surfaces from mechanical damage (i.e., wear) [7–9]. Several focused reviews have already been published on the structure of nanoconfined ILs, the dynamic behaviors of ILs in confined geometries, and the dependence of the behavior of confined ILs on several parameters, including applied potential and water content [2,7,10–12]. Despite the scientific relevance of these studies, the relatively low applied pressure (in the MPa range) in SFA and colloidal AFM experiments has not allowed gaining insights into the response of ILs upon sliding at elevated pressure (>500 MPa), i.e., under contact conditions relevant to a variety of engineering applications. Recently, the authors of the present study performed in situ AFM experiments at pressures as high as 7.3±0.4 GPa. The AFM experiments, in which a diamond-like carbon-coated silicon AFM tip was slid on air-oxidized 52100 steel in the presence of trihexyltetradecylphosphonium bis(2-ethylhexylphosphate) ($[P_{6,6,6,14}][DEHP]$) IL (Figure 1a), revealed a significant reduction of friction after removing the native passive layer from steel. Subsequent ex situ surface chemical analyses provided evidence for an increase in the lateral packing density of adsorbed alkylated phosphate ions only on metallic iron, which was attributed to the difference in adsorption configuration of phosphate ions on metallic iron (bidentate) compared to their adsorption geometry on iron oxide (monodentate). The formation of a densely packed boundary layer was proposed to be the origin of the reduction in friction measured by AFM once the native oxide layer was removed from steel [13].

As phosphonium phosphate ILs (PP-ILs) are a promising class of ILs for engine oil formulations owing to their high miscibility with mineral and synthetic oils [14], several studies

have also evaluated the lubrication mechanism of these ILs in macroscale experiments. In particular, Qu *et al.* provided evidence for the stress-assisted, thermally-activated surface reaction of PP-IL with iron to form an iron phosphate reaction layer (tribofilm) with low shear strength [15–18]. These macroscale studies apparently disagree with the aforementioned results found at the nanoscale, which highlighted that the nanoscale friction response of neat PP-ILs on iron surfaces is critically dependent on the formation of a densely-packed boundary layer made of surface-bound alkylated phosphate ions. The disagreement has been attributed to the drastically different contact conditions of the experiments: while a negligible temperature rise characterized nanoscale AFM experiments, the elevated sliding speeds together with the multi-asperity nature of macroscale contacts could increase the rate of tribochemical reactions by increasing the contact temperature (as much as 140°C above the nominal lubricant temperature) [13].

While these studies constitute a remarkable advancement in our understanding of the lubrication mechanism of ILs in general, a comprehensive understanding of the effects of contaminants and impurities (e.g., water absorbed from ambient environment, and other contaminants originated from the synthesis and processing of ILs) in ILs on their tribological performance is still lacking. These impurities are known to significantly modify the bulk and interfacial structures of ILs. For example, water can not only screen the ionic interactions in ILs by hydrogen bonding with the polar chemical groups of the ions and, thus, modify bulk properties (e.g., viscosity), but also strongly affect the IL interfacial structures [19–21] Yet, little work has been performed so far to elucidate the evolution of water-embedded IL structures at macroscale sliding contacts. Arcifa el al. have shown that water can trigger a tribochemical form of wear of silicon-based materials when it is dissolved in either hydrophilic IL (1-ethyl-3methylimidazolium ethyl sulfate) or hydrophobic IL (1-ethyl-3-methylimidazolium bis[(trifluoromethyl)sulfonyl]imide). Despite the known presence of other impurities (in addition to water) in ILs, our understanding of their influence on IL-mediated lubrication (both at the nanoscale and macroscale) has so far been elusive. In particular, halide contaminants are commonly present in ILs as many ILs are synthesized in a two-step procedure: (i) in the first step, alkyl halides are used as alkylating agents to form halide salts of desired cations; and (ii) in the second step, the halide anion is exchanged to obtain a non-halide IL using, for example, an alkali salt of the desired anion [22]. As the presence of residual halides and water molecules can

result in the formation of toxic and corrosive hydrogen halides [23,24], the determination of the level of residual halides in ILs is routinely carried out (by titration or ion chromatography) regardless of the final field of application of the ILs. Given that task-specific implementations of ILs in tribological applications hinge on their ability of meeting the ever-increasing requirements of tribological applications (*i.e.*, being effective in lubricating solid/solid contacts, while having low corrosivity), understanding the influence of halides on the tribological behavior of ILs is of paramount importance. This requires the use of surface-analytical techniques to elucidate the chemical processes occurring at sliding interfaces in the presence of ILs.

Here, we systematically evaluate the dependence of the lubricating performance of trihexyltetradecylphosphonium ($[P_{6,6,6,14}]$)-based ILs when used in 52100 steel/52100 steel contacts on the relative concentration of bis(2-ethylhexylphosphate ([DEHP]) and bromide (Br) anions. The results of surface-analytical measurements, including X-ray photoelectron spectroscopy (XPS) and time-of-flight secondary ion mass spectrometry (ToF-SIMS), are presented to elucidate the origin of changes in friction and wear behavior.

(a) (b)
$$H_{3}C(H_{2}C)_{13} (CH_{2})_{5}CH_{3} H_{3}C(H_{2}C)_{5} (CH_{2})_{5}CH_{3} H_{3}C(H_{2}C)_{5} (CH_{2})_{5}CH_{3}$$

$$O = O = O CH_{2}CH(C_{2}H_{5})CH_{2}CH_{2}CH_{2}CH_{3}$$

$$[P_{6,6,6,14}][DEHP]$$

$$[P_{6,6,6,14}]Br$$

Figure 1. Chemical structures of (a) $[P_{6,6,6,14}][DEHP]$ IL and (b) trihexyltetradecylphosphonium bromide ($[P_{6,6,6,14}]Br$) IL.

2. MATERIALS AND METHODS

The synthesis and characterization of $[P_{6,6,6,14}][DEHP]$ followed the procedure detailed by Li *et al.* [13]. The Br⁻ concentration in the as-synthesized $[P_{6,6,6,14}][DEHP]$ was measured by ion chromatography (IC, Dionex ICS-5000+ with a ICS-6000 EG, the column used was a AS11-HC-4 μ m, 4 x 250 mm and ran in a gradient of 12-60 mM KOH) and found to be 0.050±0.003%. To systematically vary the relative concentration of [DEHP] and Br⁻ anions, $[P_{6,6,6,14}]$ Br (95% purity,

Sigma Aldrich) (Figure 1b) was mixed with the synthesized $[P_{6,6,6,14}][DEHP]$ to reach Br concentrations of 3, 7, and 10 wt.% (equivalent to 0.25:1, 1:1, and 2.26:1 volume ratios of $[P_{6,6,6,14}]$ Br to $[P_{6,6,6,14}][DEHP]$. Note: the amounts of Br were intentionally designed to be larger than what would normally be present as an 'impurity' in $[P_{6,6,6,14}][DEHP]$ to elucidate their impacts in tribological performance and surface reactivity). All lubricant mixtures used for tribological tests in air were equilibrated in the ambient environment beforehand. Their water contents by weight were measured to be 15967 ± 2207 ppm by a Metrohm 917 coulometer. For the tribological test in N_2 , the $[P_{6,6,6,14}]$ Br was used as purchased and the water content was 3832 ± 320 ppm.

To evaluate the tribological performance of the ILs in the boundary-lubrication regime, reciprocating ball-on-disc experiments were performed using a Bruker UMT universal mechanical tester. Both substrates and counterparts (steel balls with a diameter of 4 mm) were made of ASTM 52100 steel (McMaster-Carr, US). The substrates were previously polished (root mean square roughness of 2.1 ± 0.4 nm measured over a scanned area of $5x5~\mu m^2$ by AFM [13]). All tribological tests were carried out with a constant normal load of 10~N, a stroke length of 4 mm, and a sliding speed of 2 mm/s. The sliding contact was immersed in the IL (or mixture of ILs) under evaluation. All tribological tests were conducted at room temperature ($296\pm1~K$) in both ambient air ($RH = 56\pm2~\%$) and N_2 environment (RH < 5%). At the end of tribological experiments, the steel samples were rinsed to remove the supernatant IL mixtures and sonicated in methanol and isopropanol for 3 min each.

To investigate the surface topography of 52100 steel substrates after tribological testing, a Wyko NT 9100 optical profilometer was employed. For each wear track, 10 line-scans across the wear track were extracted from topographic maps and, after applying a linear background, the area below the background was obtained and converted into the average specific wear rate together with the corresponding standard deviation. The wear track morphology was examined using an FEI Quanta 650 environmental scanning electron microscopy (ESEM).

To characterize the surface chemistry of steel discs used in tribological experiments, XPS and ToF-SIMS measurements were carried out. XPS analyses were performed using a Kratos Axis Ultra DLD XPS, equipped with an Al K α monochromatic X-ray source. The photoelectrons were collected with an emission angle (EA) of 90°. Areas of interest, including the wear track and non-contact area on each sample, were selected by the orthogonal camera integrated with the

XPS vacuum chamber (the camera was aligned with the photoelectron detector by parallel XPS imaging using a gold grid). XPS spectra were obtained with the incident X-ray beam of 100 µm diameter, and the power set at 120 W. For high-resolution spectra, the measurements were performed in constant-analyzer-energy (CAE) mode with a pass energy of 40 eV and a step size of 0.1 eV (full-width-at-half-maximum of the peak for Ag 3d_{5/2} is 0.77 eV). Survey spectra were collected using a pass energy of 160 eV and a step size of 1 eV. The residual pressure in the analytical chamber was below 1x10⁻⁶ Pa. The instrument was calibrated according to ISO 15472:2001 with an accuracy of ± 0.1 eV. The high-resolution spectra were processed using CasaXPS (v2.3.16, Casa Software Ltd, UK). Peak fitting was performed after background subtraction, which was carried out using an iterated Shirley-Sherwood algorithm. No sample charging was observed. The peak binding energies were referred to the aliphatic carbon signal at 285.0 eV. Quantitative analysis of XPS data was performed using the method described in Ref. [25]. Briefly, once the integrated area was obtained from fitting the original spectra after background subtraction, the quantification was performed using the first-principles method with Powell's equations [26]. The inelastic mean free path was computed using the Gries G1 formula [27].

ToF-SIMS analysis was carried out on a ToF.SIMS 5 (ION-TOF GmbH, 2010) instrument equipped with a Bi analysis gun emitting a Bi⁺ pulsed ion beam (30 keV ion energy, ~3 pA measured sample current) and a Cs sputtering gun emitting a Cs⁺ ion beam (500 eV ion energy, ~40 nA measured sample current). The analysis ion gun was set in either high current (HC) or burst alignment (BA) modes for depth profiling and in BA mode for high resolution mapping. The typical analyzed area was $100x100~\mu\text{m}^2$, raster scanned by the Bi⁺ ion beam, while for depth profiling the Cs⁺ ion beam was raster scanned over $300x300~\mu\text{m}^2$ centered around the Bi⁺ sputtered areas. All HC mode depth profiles were acquired in noninterlaced mode, *i.e.*, sequential sputtering and analysis, using a Bi₃⁺ beam for enhanced yield of large secondary ion fragments, while the BA mode depth profiles were acquired in interlaced mode, *i.e.*, simultaneous sputtering and analysis, using a Bi₁⁺ beam. All high lateral resolution maps were acquired after 10 seconds of Cs⁺ sputtering to enhance the negative polarity species and remove the adventitious material at the surface. The ToF-SIMS analysis was performed in ultra-high vacuum (~10⁻⁶ Pa). All detected ions had negative polarity and a mass resolution >5000 (m/dm). Data was processed with SurfaceLab 7.1 software package (ION-TOF GmbH, 2020).

3. RESULTS

The dependence of the tribological performance of [P_{6,6,6,14}]-based ILs when used in 52100 steel/52100 steel contacts on the relative concentration of [DEHP] and Br anions is displayed in Figure 2. While the friction coefficient does not significantly change when the $[P_{6,6,6,14}]Br/[P_{6,6,6,14}][DEHP]$ ratio was increased up to 20 % (v/v) (corresponding to a bromide content in the IL of 3 wt.%) (Figure 2a), it progressively decreases when the [P_{6,6,6,14}]Br concentration was further increased. The lowest friction was obtained with pure [P_{6,6,6,14}]Br (14 wt.% bromide content). Increasing the amount of bromide in the lubricant also leads to a significant reduction of wear (as high as 32 %) (Figure 2b). Among the computed wear coefficients, the one obtained from the experiments performed with a $[P_{6.6.6.14}]Br/[P_{6.6.6.14}][DEHP]$ ratio equal to 69 % (v/v) (corresponding to 10 wt.% bromide content in the IL) is the lowest ((2.1 \pm 0.1) x 10⁻⁶ mm³/(N·m)). Notably, while a further increase in $[P_{6,6,6,14}]Br/[P_{6,6,6,14}][DEHP]$ (from 69 v/v % to 100 v/v %) slightly increases the wear coefficient (from $(2.1 \pm 0.1) \times 10^{-6} \text{ mm}^3/(\text{N} \cdot \text{m})$ to $(2.4 \pm 0.1) \times 10^{-6} \text{ mm}^3/(\text{N} \cdot \text{m})$), the wear coefficient obtained from tests carried out using neat [P_{6,6,6,14}]Br is still significantly lower than the ones measured for the case of steel/steel contacts lubricated with ILs containing low bromide concentrations (≤ 3 wt.% or $[P_{6,6,6,14}]Br/[P_{6,6,6,14}][DEHP]$ ratio less than 20 v/v %).

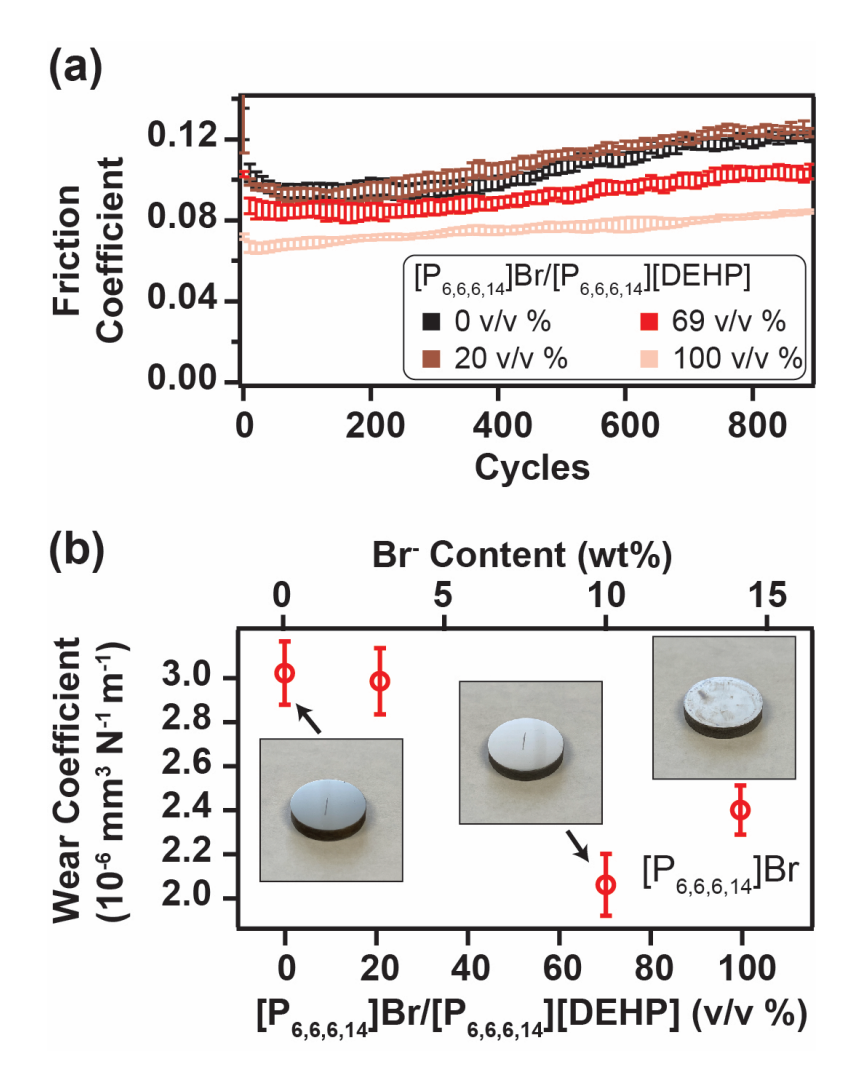


Figure 2. (a) Coefficient of friction as a function of number of cycles for a 52100 steel pin sliding on a polished 52100 steel surface in the presence of $[P_{6,6,6,14}]Br/[P_{6,6,6,14}][DEHP]$ IL mixtures; (b) wear coefficient for steel samples as a function of $[P_{6,6,6,14}]Br/[P_{6,6,6,14}][DEHP]$ volume ratio. The insets in (b) are photos of the steel samples (diameter: 14 mm) at the end of the experiments (after removing the supernatant IL and sonicating the samples with solvents).

The visual inspection of the specimens at the end of tribological tests (insets in Figure 2b) provided evidence of corrosion of the steel surface (non-contact area) only in the case of the samples used in the experiments carried out with neat $[P_{6,6,6,14}]$ Br IL. Notably, no clear signs of corrosion were observed in the case of the specimens employed for tests with ILs containing [DEHP] ions (*i.e.*, $[P_{6,6,6,14}]$ Br/ $[P_{6,6,6,14}]$ [DEHP] < 100 v/v % or $[Br^-]$ < 14 wt.%). Scanning electron microscopy (SEM) analyses of the samples (Figure 3) do not only substantiate these observations, but also allow for changes in wear mechanism with bromide content in the IL

mixture to be identified: while the morphology of the tracks generated on steel surfaces lubricated with ILs with [DEHP] ions (*i.e.*, [P_{6,6,6,14}]Br/[P_{6,6,6,14}][DEHP] < 100 v/v % or [Br⁻] < 14 wt.%) indicate an abrasive wear mechanism (Figure 3a and 3b), the presence of debris and small pits within the wear track on the sample lubricated with neat [P_{6,6,6,14}]Br (Figure 3c) suggests an abrasive/corrosive form of wear.

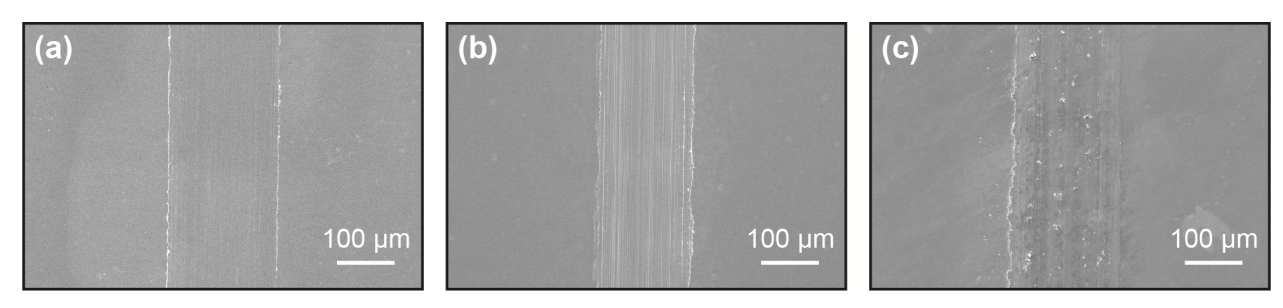


Figure 3. SEM images of wear tracks on 52100 steel samples after tribological testing in the presence of: (a) as synthesized $[P_{6,6,6,14}][DEHP]$ IL (0.05 wt.% $[Br^-]$); (b) 50/50 v/v % $[P_{6,6,6,14}][DEHP]/[P_{6,6,6,14}]Br$ (7 wt.% $[Br^-]$); and (c) neat $[P_{6,6,6,14}]Br$ (14 wt.% $[Br^-]$).

To understand the chemical origin of the variation in tribological performance and surface morphology, ex situ XPS measurements were conducted on the specimens after tribological testing. Figure 4 displays the high-resolution phosphorus 2p (P 2p) spectra obtained from wear tracks and non-contact areas of samples used in tribotests performed with as synthesized $[P_{6.6.6.14}][DEHP] \ IL \ (0.05 \ wt.\% \ [Br^-]), \ 50/50 \ v/v \ [P_{6,6,6,14}][DEHP]/[P_{6,6,6,14}]Br \ (7 \ wt.\% \ [Br^-]), \ and \ (1.005 \ wt.\% \ [Br^-]),$ neat $[P_{6,6,6,14}]$ Br (14 wt.% [Br-]). As the P 2p signal is the convolution of $2p_{3/2}$ and $2p_{1/2}$ components due to spin-orbit coupling, curve synthesis was performed using two signals having area ratio equal to 0.5 and energy separation equal to 0.85 eV. The XPS P 2p signals shown in Figure 4 were fitted on the basis of XPS data acquired using the same experimental conditions on pure $[P_{6,6,6,14}][DEHP]$ and $[P_{6,6,6,14}]Br$ ILs, which provide reference values for the binding energies of $[P_{6,6,6,14}]$ (2p_{3/2} at 132.5±0.1 eV) and [DEHP] (2p_{3/2} at 133.6±0.1 eV) (see table S1 in the Supporting Information). Upon fitting the XPS P 2p acquired in the non-contact region of steel surfaces used in tribological experiments performed with as synthesized $[P_{6,6,6,14}][DEHP]$ IL (0.05 wt.% [Br-]) (Figure 4a) and 50/50 v/v [P_{6,6,6,14}][DEHP]/[P_{6,6,6,14}]Br (7 wt.% [Br-]) (Figure 4b), a shift of the characteristic binding energy assigned to the $[P_{6,6,6,14}]$ and [DEHP] ions was detected. This can be attributed to a change in phosphorus partial charge in both [P_{6,6,6,14}]

and [DEHP] adsorbed on steel surfaces. Notably, no significant difference was observed between the spectra acquired in the wear track and those collected in the non-contact area. In the case of the specimen lubricated with neat [P_{6.6,6,14}]Br (Figure 4c), the P 2p signals in the wear track and non-contact area could not be fitted with a single component that could be assigned to $[P_{6,6,6,14}]$ cations, but an additional doublet had to be introduced at higher binding energy (2p_{3/2} at 133.5 \pm 0.1 eV in the wear track and 2p_{3/2} at 133.6 \pm 0.1 eV in the non-contact area). The detection of this new doublet at higher binding energy in the XPS P 2p spectra collected on steel specimen used in tribotests performed with neat $[P_{6,6,6,14}]$ Br is indicative of the formation, in the nearsurface region of steel, of phosphorus-containing species in which phosphorus atoms have a higher partial positive charge compared to the phosphorus atoms in $[P_{6,6,6,14}]$ ions. As the new doublet has similar binding energy as the one of [DEHP] anions adsorbed on the surface of specimens employed for tests carried out with either as synthesized $[P_{6,6,6,14}][DEHP]$ IL (0.05 wt.% [Br-]) (Figure 4a) or 50/50 v/v [P_{6,6,6,14}][DEHP]/[P_{6,6,6,14}]Br (7 wt.% [Br-]), this new spectral feature could be assigned to phosphorus atoms bonded to oxygen. This finding suggests that when neat $[P_{6,6,6,14}]$ Br is used to lubricate steel/steel sliding contacts, phosphonium cations undergo a bond-breaking process leading to the formation of phosphorus-oxygen moieties.

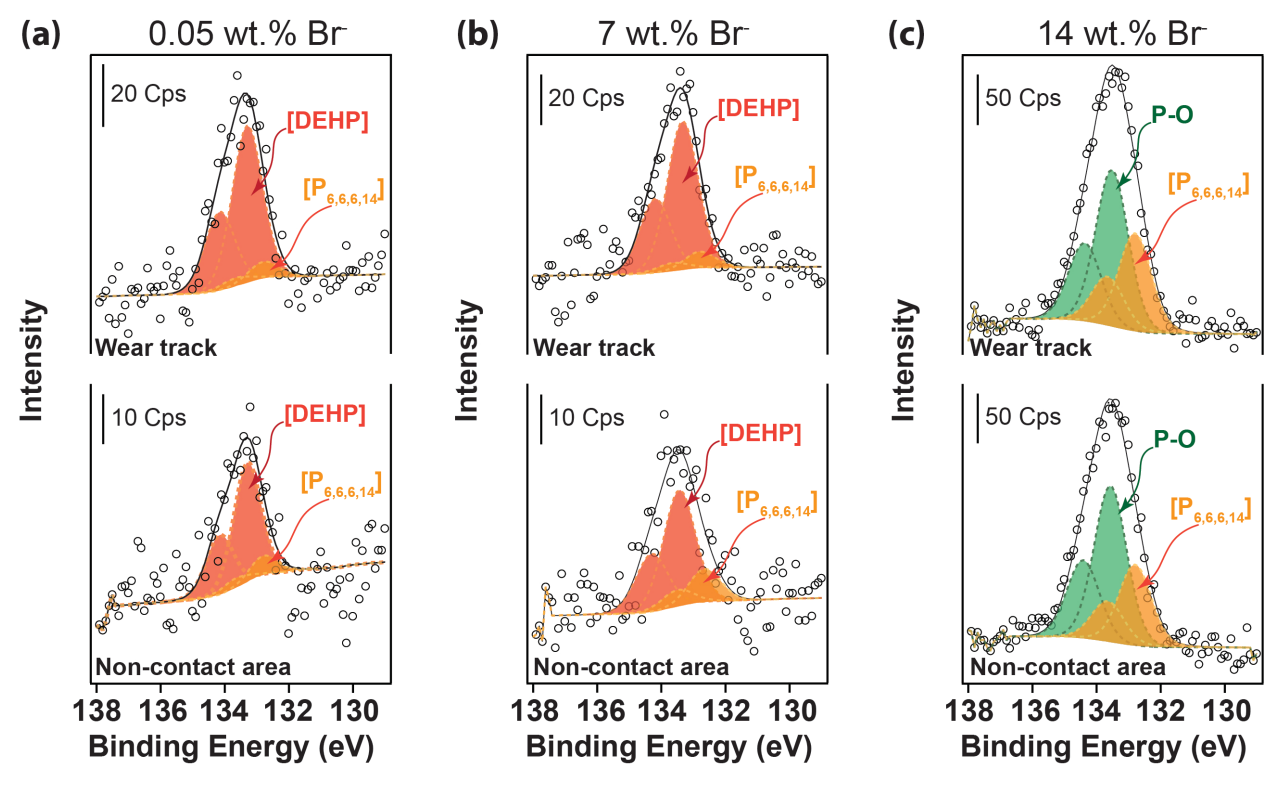


Figure 4. High-resolution XPS phosphorus 2p spectra obtained from the wear tracks and non-contact areas of samples used in tribological experiments performed in the presence of: (a) as synthesized $[P_{6,6,6,14}][DEHP]$ IL (0.05 wt.% [Br]); (b) $50/50 \text{ v/v \% [P_{6,6,6,14}][DEHP]/[P_{6,6,6,14}]Br}$ (7 wt.% [Br]); and (c) neat $[P_{6,6,6,14}]Br$ (14 wt.% [Br]).

The ratio of phosphorus to iron ([P]/[Fe]) estimated by XPS (using the P 2p and Fe 2p signals. The Fe 2p spectra are shown in Figure S2 in the Supporting Information) was found to be significantly higher in both wear track and non-contact area of the samples used for the experiments performed with neat $[P_{6,6,6,14}]$ Br compared to the [P]/[Fe] ratios computed from the data acquired on samples employed in experiments with ILs containing [DEHP] ions (*i.e.*, $[P_{6,6,6,14}]$ Br/ $[P_{6,6,6,14}]$ [DEHP] < 100 v/v % or $[Br^-]$ < 14 wt.%), as shown in Figure 5. Although the XPS spectra do not indicate any significant, tribologically-induced difference in the elements' bonding configurations in the wear track relative to the non-contact region, the [P]/[Fe] ratio shows subtle changes caused by mechanical sliding. As for the experiments carried out with as synthesized $[P_{6,6,6,14}]$ [DEHP] IL (0.05 wt.% $[Br^-]$) and 50/50 v/v $[P_{6,6,6,14}]$ [DEHP]/ $[P_{6,6,6,14}]$ Br (7 wt.% $[Br^-]$), the [P]/[Fe] ratios obtained from spectra collected in the wear tracks are higher than the ratios obtained from the data acquired in the non-contact

areas. Conversely, in the case of the steel specimen used in sliding tests carried out with neat $[P_{6,6,6,14}]Br$, the non-contact area exhibits a higher [P]/[Fe] ratio than the wear track.

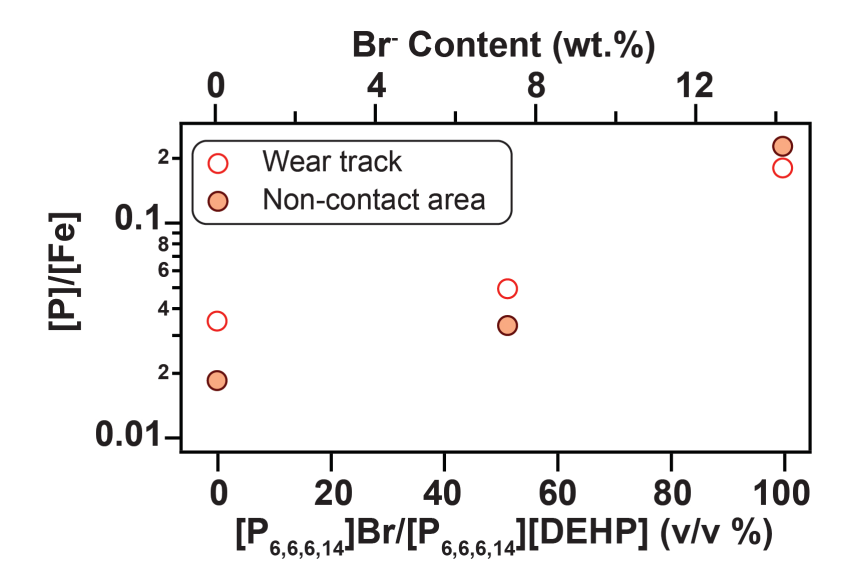


Figure 5. Phosphorus-to-iron ([P]/[Fe]) ratio as a function of bromide content computed from XPS analyses performed on sample surfaces used in tribological experiments carried out in the presence of $[P_{6,6,6,14}]Br/[P_{6,6,6,14}][DEHP]$ IL mixtures.

To gain further insights into any potential change in the molecular structure of ILs upon sliding, high lateral resolution imaging and depth-profiling ToF-SIMS analyses were performed. These measurements allowed for the evaluation of the lateral and vertical distribution of chemical compounds in the near-surface region of steel specimens after tribological testing. Figure 6 shows the chemical maps of selected ionized fragments detected at the boundaries of the wear tracks. In the PO₂⁻ maps collected on samples used for tests carried out with as synthesized [P_{6,6,6,14}][DEHP] IL (0.05 wt.% [Br⁻]) and 50/50 v/v [P_{6,6,6,14}][DEHP]/[P_{6,6,6,14}]Br (7 wt.% [Br⁻]), a higher yield of PO₂⁻ secondary ion fragments could be found in the wear tracks compared to the non-contact areas, which is consistent with the XPS results presented above. As for the samples that were lubricated with neat [P_{6,6,6,14}]Br, PO₂⁻ fragments could be detected in both the wear track and non-contact area. This analytical result corroborates our XPS data in Figure 4, as it provides evidence for the chemical transformation of phosphonium cations. Additionally, although the ToF-SIMS results suggest a higher amount of PO₂⁻ fragments inside the wear track generated in the presence of neat [P_{6,6,6,14}]Br than in the non-contact area, a

substantial amount of the same fragment was found in the non-contact area, which is not the case for samples lubricated by as synthesized $[P_{6,6,6,14}][DEHP]$ IL (0.05 wt.% [Br]) and 50/50 v/v $[P_{6,6,6,14}][DEHP]/[P_{6,6,6,14}]Br$ (7 wt.% [Br]). The increased yield of phosphorus-containing species in the non-contact area of the sample lubricated with neat $[P_{6,6,6,14}]Br$ IL compared to the non-contact areas of the samples used in tribological experiments performed in the presence of ILs containing [DEHP] ions $(i.e., [P_{6,6,6,14}]Br/[P_{6,6,6,14}][DEHP] < 100 \text{ v/v \% or } [Br] < 14 \text{ wt.\%})$ corroborates the higher [P]/[Fe] ratio computed from XPS data acquired on the non-contact area (Figure 5).

The ToF-SIMS results also display a clear contrast in the lateral distribution of bromide (Figure 6b). Independently of the content of bromide in the IL used in the tribological tests, the Br maps show an increased amount of Br in the wear tracks relative to the non-contact region. However, this effect is less pronounced for specimens used in experiments carried out with assynthesized [P_{6,6,6,14}][DEHP] IL (0.05 wt.% [Br]), while for the other two samples used in sliding experiments with ILs having higher bromide content IL (7 wt.% and 14 wt.% [Br]), the yield of Br fragments is much higher. A similar result could be found when considering FeBr fragments (Figure S3).

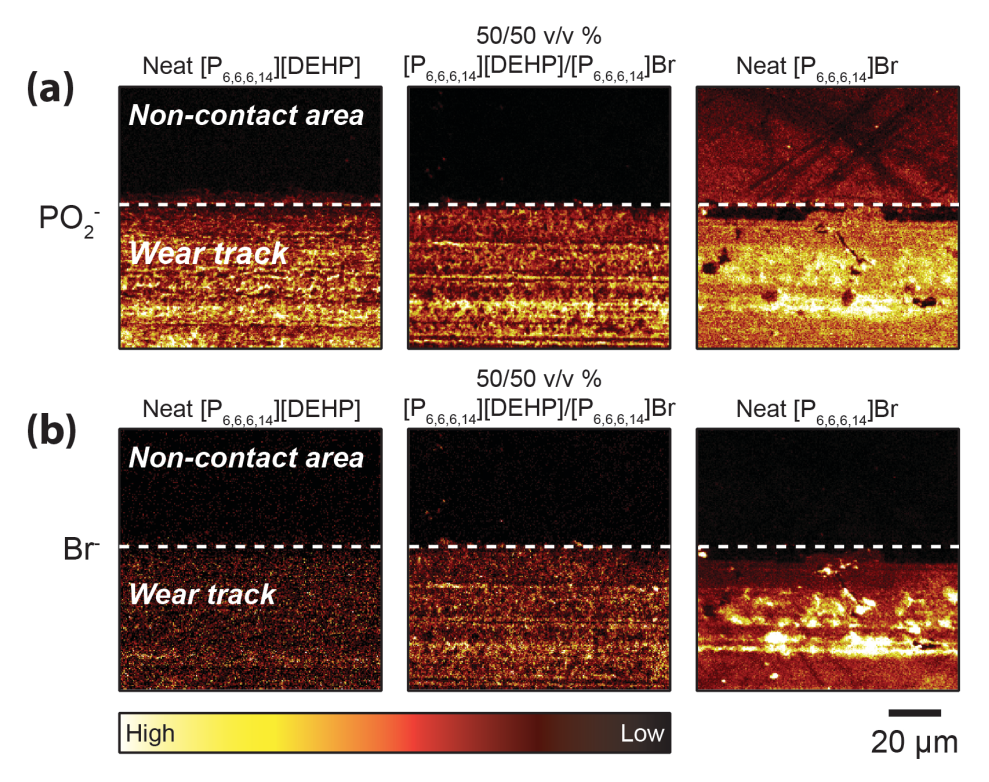


Figure 6. ToF-SIMS chemical maps of PO_2^- (a) and Br^- (b) acquired at the boundaries between wear tracks and non-contact areas of steel samples after tribological tests performed in the presence of as synthesized [$P_{6,6,6,14}$][DEHP] IL (0.05 wt.% [Br^-]), 50/50 v/v [$P_{6,6,6,14}$][DEHP]/[$P_{6,6,6,14}$]Br (7 wt.% [Br^-]), and neat [$P_{6,6,6,14}$]Br (14 wt.% [Br^-]). The white dashed lines in the maps label the borderlines between wear tracks and non-contact areas. All maps show a 100 x 100 μm^2 area.

To evaluate the vertical distribution of molecular fragments detected in the near-surface region of steel specimens after tribological testing, standard depth profiles (non-interlaced, HC modes) of several ionized fragments were acquired (Figure 7). For PO and FeBr fragments, their yields decreased with sputtering depth much more quickly in the non-contact regions than in the wear tracks (independently of the bromide content of the IL used in tribological tests). This result indicates the mechanically-induced, surface-to-bulk transport (*i.e.*, mechanical mixing) of IL ions and/or their fragments. It has to be highlighted that in the case of FeBr fragments, increasing the amount of bromide in the IL mixture used in tribological experiments increases both the yield of FeBr fragments detected in depth-profiles and the extent of the surface-to-bulk transport of IL ions and/or their fragments, as demonstrated by the increased depth to which FeBr fragments are transported when using ILs containing larger amounts of bromide ions.

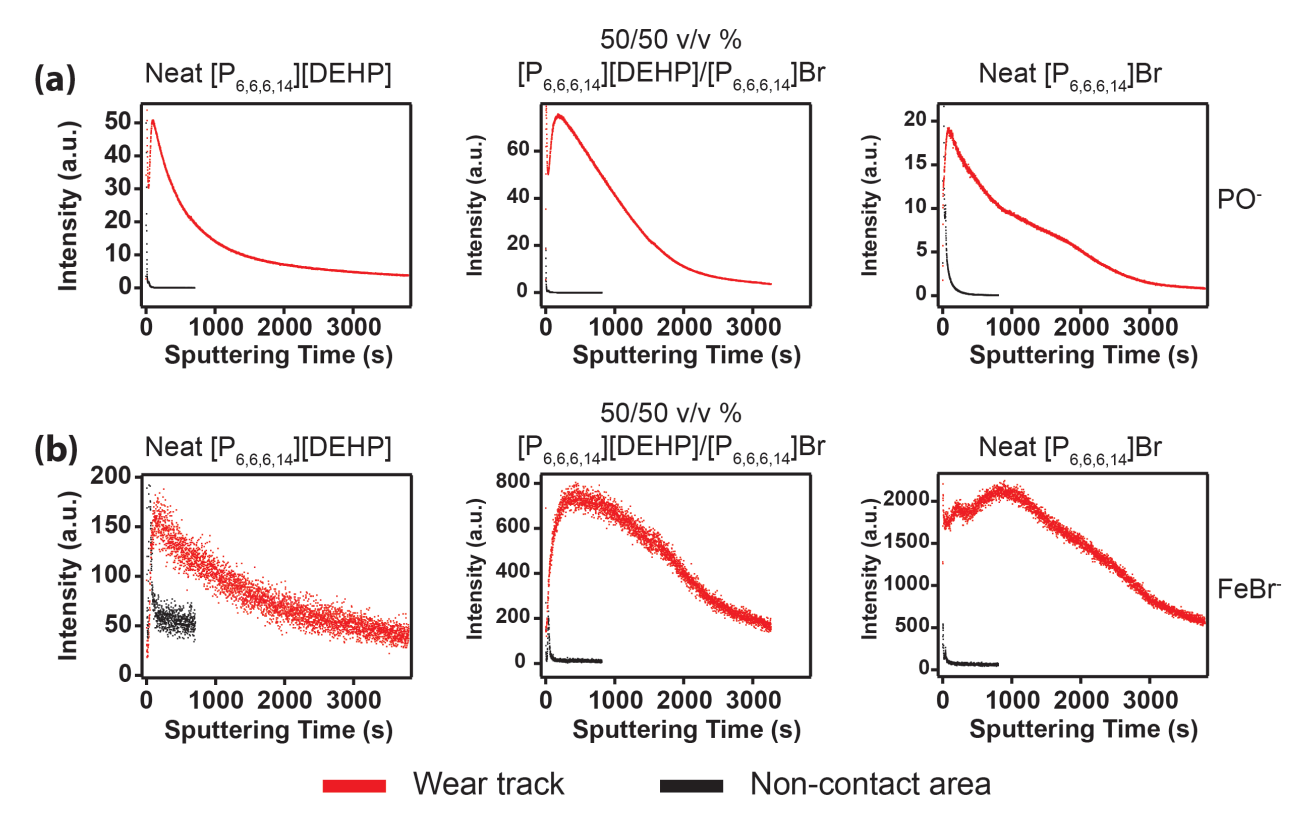


Figure 7. Depth profiles (wear tracks (red) and non-contact areas (black)) obtained from ToF-SIMS measurements conducted on steel specimens used for tribological tests performed in the presence of as synthesized $[P_{6,6,6,14}][DEHP]$ IL (0.05 wt.% $[Br^-]$), 50/50 v/v $[P_{6,6,6,14}][DEHP]/[P_{6,6,6,14}]Br$ (7 wt.% $[Br^-]$), and neat $[P_{6,6,6,14}]Br$ (14 wt.% $[Br^-]$). Depth profiles include ionized fragments PO^- (a) and $FeBr^-$ (b) from the wear tracks and non-contact areas.

The rendered three-dimensional (3D) spatial distributions of PO_2^- and Br^- for high lateral resolution depth profiles (interlaced, BA mode) are displayed in Figure 8. While in the case of wear tracks generated on steel specimens in the presence of ILs containing [DEHP] ions (*i.e.*, $[P_{6,6,6,14}]Br/[P_{6,6,6,14}][DEHP] < 100 \text{ v/v} \% \text{ or } [Br^-] < 14 \text{ wt. } \%$), the 3D renderings indicate a homogeneous depth distribution of PO_2^- and Br^- , in the case of the wear tracks formed in experiments carried out with neat $[P_{6,6,6,14}]Br$ (14 wt.% $[Br^-]$), the 3D rendering suggests a significant surface-to-bulk transport of bromide together with the generation of a near-surface layer rich in PO_2^- . Additionally, the ToF-SIMS data provide evidence for a much larger surface coverage of PO_2^- fragments in the non-contact region of steel specimens used in tests performed with neat $[P_{6,6,6,14}]Br$ than the surface coverage of PO_2^- fragments in the non-contact area of

samples employed in experiments carried out with ILs containing [DEHP] ions (*i.e.*, $[P_{6,6,6,14}]Br/[P_{6,6,6,14}][DEHP] < 100 \text{ v/v }\% \text{ or } [Br^-] < 14 \text{ wt.}\%$).

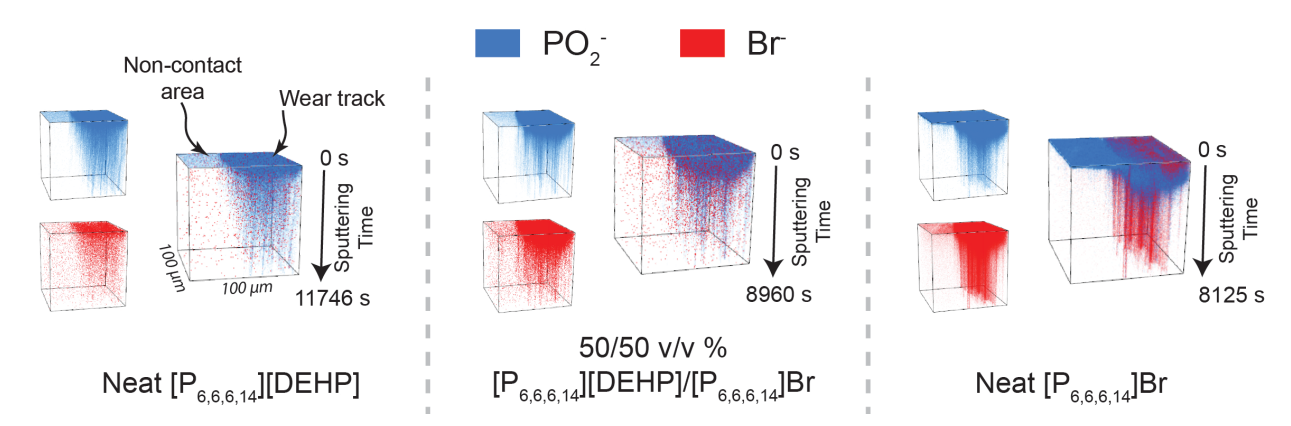


Figure 8. Three-dimensional (3D) rendering of the distribution of PO₂⁻ and Br⁻ fragments determined on the basis of ToF-SIMS high lateral resolution depth profiles.

To evaluate the extent of the chemically-modified surface region created upon sliding in the presence of ILs, ToF-SIMS depth profiles of Fe₄⁻ were also acquired (Figure 9). As for the noncontact regions, the Fe₄⁻ profiles reach steady-state very quickly independently of the bromide content in the IL mixtures. Conversely, a much longer sputtering time is required for the Fe₄⁻ fragments to achieve a constant intensity in the wear track, thus indicating the mechanically assisted formation of a chemically modified layer in the near-surface region of steel upon sliding in the presence of the ILs under investigation. Notably, upon increasing the bromide content in the IL used in tribological tests, the sputtering time required to achieve steady-state intensity in the Fe₄⁻ profile increases, which suggests an increase in the thickness of the chemically modified surface layer within the wear track with the bromide content in the IL.

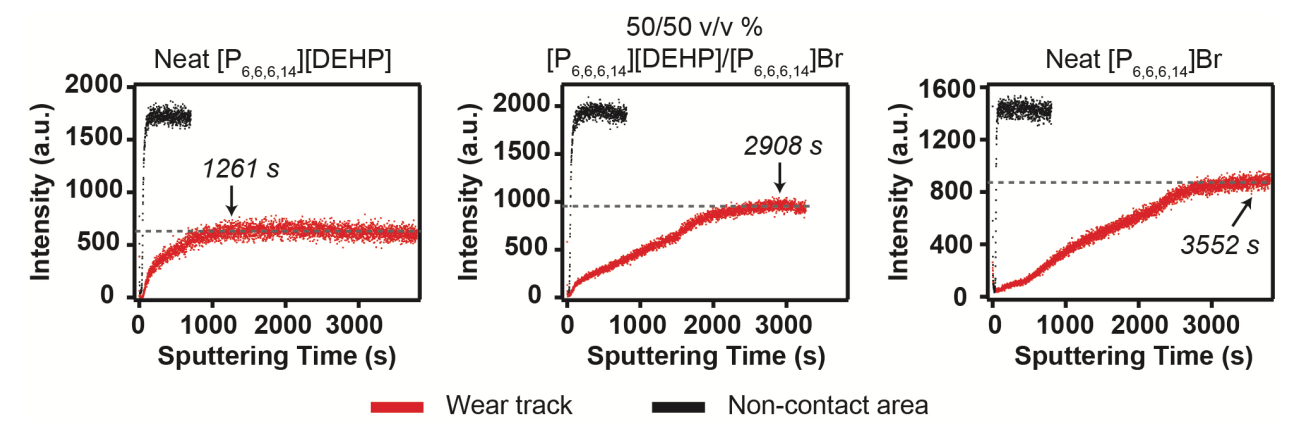


Figure 9. ToF-SIMS depth profiles of Fe₄⁻ (wear tracks (red) and non-contact areas (black)) from ToF-SIMS measurements conducted on steel specimens used for tribological tests performed in the presence of as synthesized [P_{6,6,6,14}][DEHP] IL (0.05 wt.% [Br⁻]), 50/50 v/v [P_{6,6,6,14}][DEHP]/[P_{6,6,6,14}]Br (7 wt.% [Br⁻]), and neat [P_{6,6,6,14}]Br (14 wt.% [Br⁻]). The grey dashed lines indicate the steady-state intensity of each profile. The approximate sputtering times at which the profiles reach constant intensity are presented. The significant gap of the steady-state intensity between the contact and non-contact areas is largely due to the topographic differences.

4. DISCUSSION

The results of the tribological experiments presented in this study highlight the dependence of the lubricating properties of $[P_{6,6,6,14}]$ -based ILs on the relative concentration of [DEHP] and Br anions. More specifically, the coefficient of friction and wear coefficient indicated that the tribological response of $[P_{6,6,6,14}]$ -based ILs when used to lubricate steel/steel contacts is not significantly affected upon increasing the $[P_{6,6,6,14}]$ Br/ $[P_{6,6,6,14}]$ DEHP] ratio up to 20 % (v/v) (corresponding to a bromide content in the IL of 3 wt.%). While a further increase in $[P_{6,6,6,14}]$ Br/ $[P_{6,6,6,14}]$ [DEHP] ratio (>20 % (v/v)) leads to a reduction of friction and wear, it is critical to highlight that corrosion products appeared on the surface of steel samples (non-contact regions) only in tribological tests performed with neat $[P_{6,6,6,14}]$ Br. These findings do not only demonstrate the possibility of employing $[P_{6,6,6,14}]$ [DEHP] IL containing significant amounts of bromide for lubricating steel/steel contacts without any potential corrosion issues, but also indicate that the tribological behavior of $[P_{6,6,6,14}]$ -based IL can be tuned by varying the ratio of

[DEHL] and bromide anions in the IL. This result opens the path towards the task-specific implementation of phosphonium-based IL in tribological applications.

Insights into the mechanisms underpinning this variation in tribological behavior and surface reactivity of $[P_{6,6,6,14}][DEHP]/[P_{6,6,6,14}]Br$ IL mixtures could be obtained by *ex situ* analyses. XPS and ToF-SIMS measurements performed on steel specimens used in tribological experiments carried out in the presence of as synthesized $[P_{6,6,6,14}][DEHP]$ IL revealed an increase in phosphorus content in the contact region (wear track) relative to the non-contact area. This finding is in agreement with our previous work, which indicated an increase in coverage of [DEHP] ions adsorbed on steel surfaces once the native oxide is mechanically removed.[13] However, while in the case of our previous experiments $[P_{6,6,6,14}][DEHP]$ IL contained a limited amount of absorbed water, the significant water content $(15967 \pm 2207 \text{ ppm})$ in the ILs used in the present work could lead to the formation of hydrobromic acid, whose reaction with iron and iron oxide is thermodynamically favorable [28]:

$$Fe_3O_4 + 9HBr \rightarrow 3FeBr_3 + 4H_2O + \frac{1}{2}H_2$$
 $\Delta G_R^0 = -26.4 \ kcal$ $Fe_2O_3 + 6HBr \rightarrow 2FeBr_3 + 3H_2O$ $\Delta G_R^0 = -25.7 \ kcal$ $Fe + 3HBr \rightarrow FeBr_3 + \frac{3}{2}H_2$ $\Delta G_R^0 = -19.7 \ kcal$

The absence of any corrosion products together with the detection of trace amounts of Br and FeBr fragments in the non-contact region of steel samples used in experiments performed with ILs containing 0.05 wt.% and 7 wt.% [Br] (respectively corresponding to as synthesized [P6,6,6,14][DEHP] IL and 50/50 v/v [P6,6,6,14][DEHP]/[P6,6,6,14]Br) suggests that [DEHP] ions act as a corrosion inhibitor by adsorbing on the steel surface. However, the removal of surface adsorbed [DEHP] ions in the contact area by the sliding steel pin continuously exposes iron and iron oxide to hydrobromic acid, thus leading to the formation of iron bromide, as indicated by ToF-SIMS data. The chemical transformation of phosphonium cations and the formation of phosphorus-oxygen moieties in the non-contact area on samples lubricated by [P6,6,6,14]Br suggest that phosphonium cations are hydrolyzed by water at steel/IL interface in the absence of [DEHP] anions. As reported in the literature, the multi-step hydrolysis reaction of phosphonium

salts results in the formation of phosphine oxide [29–31], which can be further hydrolyzed to generate additional P-O bonds (Figure 10) [32].

Figure 10. Hydrolysis reaction of phosphonium salts.

The products with phosphorus-oxygen species could adsorb on iron and iron oxides, as suggested by XPS and ToF-SIMS results. The significant amounts of water molecules generated during the corrosion reaction could also enhance the hydrolysis of phosphonium/phosphine oxide and the generation of a phosphorus-rich boundary layer, which is proposed to cause a decrease in steel-steel adhesion and interfacial shear strength, thus explaining the measured decrease in friction and wear with bromide content (Figure 2).

In the case of neat [P_{6,6,6,14}]Br IL, the corrosion of steel by hydrobromic acid results in the formation of brown products in the non-contact region (inset in Figure 2b) together with a change in the wear mechanism (Figure 3). While the shear-induced, surface-to-bulk transport of iron bromide leads to the generation of a thick, near-surface region (Figure 9) that can aid in wear reduction, the hydrolysis of phosphonium ions generates significant amounts of phosphorus-oxygen bonds in both the contact and non-contact regions, which increases the surface coverage of phosphorus-containing fragments in both regions as indicated by the phosphorus-to-iron ratio computed from XPS data (Figure 5).

Altogether the results of *ex situ* analytical measurements suggest that the lubricating performance of [P_{6,6,6,14}]-based ILs with systematically varied relative concentration of [DEHP] and Br⁻ anions is a balance between corrosivity and surface reactivity: while [DEHP] ions in the IL is critical to inhibit the corrosion of steel in the non-contact region, the formation of species containing surface functional (phosphorus-oxygen) groups as a result of the hydrolysis of phosphonium ions enhanced by the generation of water at the steel/IL interface increases the surface coverage of phosphorus, which decreases friction by decreasing adhesion at steel/steel contacts and lowering the interfacial shear strength.

To provide further experimental evidence for the key role of water at the steel/IL interface in the formation of hydrobromic acid with the subsequent corrosion reaction of steel, control tribological experiments were performed using neat $[P_{6,6,6,14}]$ Br in dry nitrogen under the same experimental conditions of the tests described above (water content in $[P_{6,6,6,14}]$ Br equal to 3832 ± 320 ppm). The friction results indicated a lower coefficient of friction in the experiment carried out in nitrogen than the friction coefficient obtained in the test carried out in ambient air. Notably, the visual inspection of the steel specimen at the end of the experiment performed in nitrogen did not show any clear sign of corrosion (inset of Figure 11a), thus demonstrating the key role of water at the steel/ $[P_{6,6,6,14}]$ Br IL interface in triggering the corrosion of steel.

The ToF-SIMS chemical maps acquired on the sample used in experiments performed in the presence of $[P_{6,6,6,14}]$ Br IL in dry environment indicated the presence of Br inside the wear track (Figure 11b) together with PO_2 fragments. These fragments still originate from the formation of hydrobromic acid due to the presence of even small amounts of water in the environment. While the reaction of HBr and iron results in additional water molecules, which add to the water at the interface and hydrolyze phosphonium ions, the amounts of iron bromide and phosphorus-oxygen moieties (detected as PO^- or PO_2 fragments) of the sample used for experiments performed in N_2 is significantly lower than those measured on samples tested in ambient air (Figure 11c). The lower friction coefficient measured in experiments performed in dry environments could be explained on the basis of the smaller thickness of iron bromide formed in the contact area. As demonstrated by Gao *et al.*, an increase in friction occurs with the thickness of inorganic halide films on iron either due to enlarged contact areas (thickness < 0.3 μ m, following Amontons' law), or elasticity for thicker films (> 0.3 μ m) [33,34].

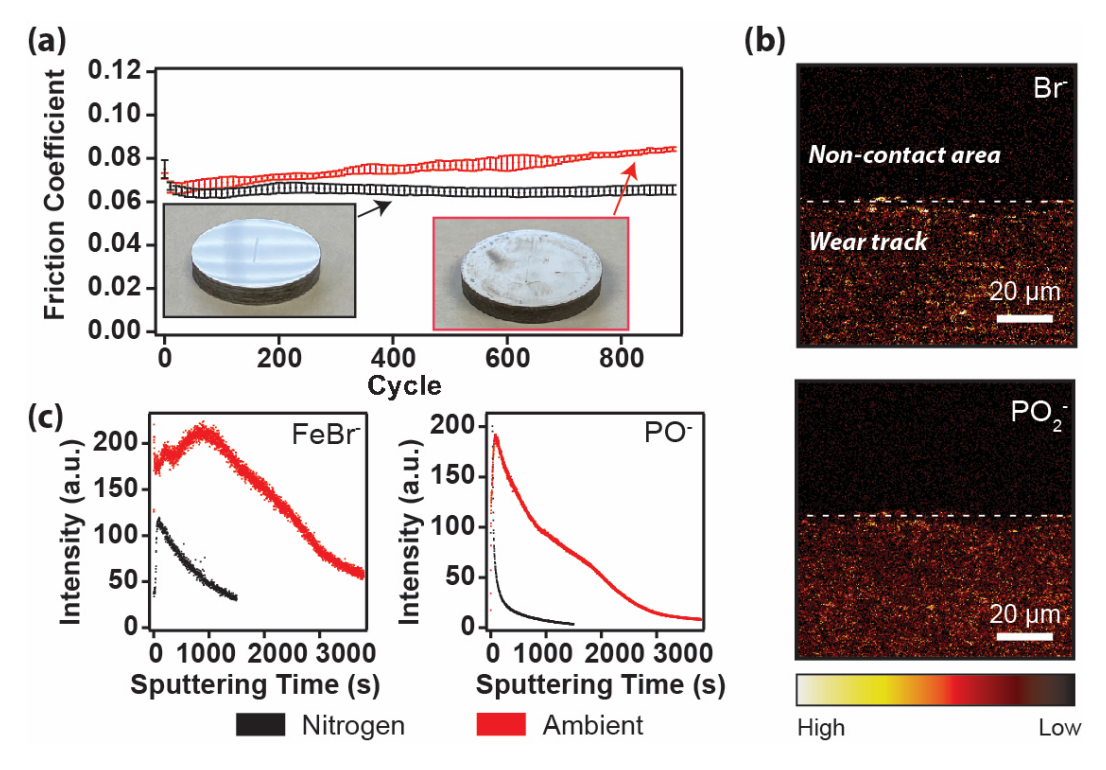


Figure 11. (a) Coefficient of friction as a function of the number of cycles for a 52100 steel pin sliding on a polished 52100 steel substrate in the presence of neat $[P_{6,6,6,14}]Br$ IL in a dry environment (N_2) and ambient air. The insets show photos of the steel samples at the end of the experiments (after removing the supernatant IL). The samples have diameters of 14 mm; (b) ToF-SIMS chemical maps of Br^- and PO_2^- fragments at the boundary of the wear track and noncontact area of the sample lubricated by $[P_{6,6,6,14}]Br$ in N_2 . White dashed lines in (b) are the approximate borderline between the wear track and non-contact area; (c) ToF-SIMS depth profiles of FeBr $^-$ and PO $^-$ fragments extracted from the wear tracks of samples lubricated by $[P_{6,6,6,14}]Br$ in ambient air (red), and N_2 (black).

5. CONCLUSION

The lubricating performance of $[P_{6,6,6,14}]$ -based ILs when used in steel/steel contacts was systematically evaluated as a function of the relative concentration of [DEHP] and Br^- anions. The tribological results highlighted that no significant changes in the coefficient of friction and wear coefficient occurred upon increasing the $[P_{6,6,6,14}]$ Br-to- $[P_{6,6,6,14}]$ [DEHP] volume ratio up to 0.2:1, while a further increase in the $[P_{6,6,6,14}]$ Br-to- $[P_{6,6,6,14}]$ [DEHP] volume ratio leads to a reduction of friction and wear. The results of *ex situ* analytical measurements indicated that the dependence of the lubricating performance of $[P_{6,6,6,14}]$ -based ILs on the Br-to-[DEHP] anion

ratio originates from the balance between corrosivity and surface reactivity of the IL: while [DEHP] ions inhibit the corrosion of steel in the non-contact region, the formation of species containing surface functional (phosphorus-oxygen) groups as a result of the hydrolysis of phosphonium ions enhanced by the reaction of hydrobromic acid (formed by the presence of significant amounts of water at the IL/steel interface) with steel increases the surface coverage of phosphorus, which decreases friction by decreasing adhesion at steel/steel contacts and lowering the interfacial shear strength.

These findings demonstrate that the tribological properties of phosphonium-based IL can be effectively tuned by varying the amount of bromide in the IL while maintaining high corrosion resistance in the presence of [DEHP], thus opening the path towards the adjustable and even task-specific implementation of [P_{6.6.6.14}][DEHP] IL in tribological applications.

ASSOCIATED CONTENT

High-resolution XPS P 2p spectra of neat $[P_{6,6,6,14}][DEHP]$ IL and $[P_{6,6,6,14}]Br$ IL; fitting parameters for the high-resolution XPS P 2p spectra acquired on steel samples used in tribological experiments performed in the presence of $[P_{6,6,6,14}][DEHP]$ IL with systematically varied amount of Br⁻; high-resolution XPS Fe 2p spectra acquired on steel samples used in tribological experiments performed in the presence of $[P_{6,6,6,14}][DEHP]$ IL with systematically varied amount of Br⁻; ToF-SIMS chemical maps of FeBr⁻ acquired at the boundaries between wear tracks and non-contact areas of steel samples after tribological tests performed in the presence of $[P_{6,6,6,14}][DEHP]$ IL containing systematically varied bromide content; wear coefficients and wear track cross-sections of steel samples used in tribological experiments carried out with $[P_{6,6,6,14}]$ Br IL in ambient air $(RH = 56 \pm 2 \%)$ and N_2 environment (RH < 5%).

AUTHOR INFORMATION

Corresponding Author

* Email: filippo.mangolini@austin.utexas.edu

Notes

The authors declare no competing financial interests.

CREDIT AUTHORSHIP CONTRIBUTION STATEMENT

Zixuan Li: Conceptualization, Investigation, Data curation, Formal analysis, Writing - original draft, Writing - review & editing; Hugo Celio: Investigation, Formal analysis, Writing - review & editing; Nicolás Molina: Investigation, Formal analysis, Data curation, Writing - review & editing; Jude Kershaw: Investigation, Formal analysis; Oscar Morales-Collazo: Investigation, Formal analysis; Joan F. Brennecke: Conceptualization, Investigation, Formal analysis, Writing - review & editing; Filippo Mangolini: Conceptualization, Investigation, Formal analysis, Writing - original draft, Funding acquisition, Writing - review & editing.

ACKNOWLEDGMENT

The material is based upon work supported by the Welch Foundation (Grant No. F-2002-20190330), the National Science Foundation Faculty Early Career Development Program (Grant No. 2042304), and the Taiho Kogyo Tribology Research Foundation (Grant No. 20A03). F.M. acknowledges support from the 2018 Ralph E. Powe Junior Faculty Enhancement Award sponsored by the Oak Ridge Associated Universities (ORAU), and from the Walker Department of Mechanical Engineering and the Texas Materials Institute at the University of Texas at Austin.

REFERENCES

- [1] C. Ye, W. Liu, Y. Chen, L. Yu, N. Si, Room-temperature ionic liquids: a novel versatile lubricant, Chem. Commun. (2001) 2244–2245. https://doi.org/10.1039/B106935G.
- [2] R.M. Espinosa-Marzal, M. Han, A. Arcifa, N.D. Spencer, A. Rossi, Ionic Liquids at Interfaces and Their Tribological Behavior, in: Ref. Modul. Chem. Mol. Sci. Chem. Eng., 2017. https://doi.org/10.1016/B978-0-12-409547-2.13857-0.
- [3] A. Arcifa, A. Rossi, S.N. Ramakrishna, R. Espinosa-Marzal, A. Sheehan, N.D. Spencer, Lubrication of Si-Based Tribopairs with a Hydrophobic Ionic Liquid: The Multiscale Influence of Water, J. Phys. Chem. C. 122 (13) 7331–7343. https://doi.org/10.1021/acs.jpcc.8b01671.
- [4] A. Suzuki, Y. Shinka, M. Masuko, Tribological characteristics of imidazolium-based room temperature ionic liquids under high vacuum, Tribol. Lett. 27 (2007) 307–313. https://doi.org/10.1007/s11249-007-9235-8.
- [5] I. Minami, H. Kamimura, S. Mori, Thermo-oxidative stability of ionic liquids as lubricating fluids, J. Synth. Lubr. 24 (2007) 135–147. https://doi.org/10.1002/jsl.36.
- [6] S. Zhang, J. Zhang, Y. Zhang, Y. Deng, Nanoconfined Ionic Liquids, Chem. Rev. 117 (2017) 6755–6833. https://doi.org/10.1021/acs.chemrev.6b00509.
- [7] R. Lhermerout, C. Diederichs, S. Perkin, Are Ionic Liquids Good Boundary Lubricants? A Molecular Perspective, Lubricants. 6 (1). https://doi.org/10.3390/lubricants6010009.
- [8] S. Perkin, T. Albrecht, J. Klein, Layering and shear properties of an ionic liquid, 1-ethyl-3-methylimidazolium ethylsulfate, confined to nano-films between mica surfaces, Phys. Chem. Chem. Phys. 12 (2010) 1243–1247. https://doi.org/10.1039/b920571c.
- [9] P.K. Cooper, C.J. Wear, H. Li, R. Atkin, Ionic Liquid Lubrication of Stainless Steel: Friction is Inversely Correlated with Interfacial Liquid Nanostructure, ACS Sustain. Chem. Eng. 5 (2017) 11737–11743. https://doi.org/10.1021/acssuschemeng.7b03262.
- [10] A. Somers, P. Howlett, D. MacFarlane, M. Forsyth, A Review of Ionic Liquid Lubricants, Lubricants. 1 (2013) 3–21. http://www.mdpi.com/2075-4442/1/1/3.
- [11] J. Sweeney, F. Hausen, R. Hayes, G.B. Webber, F. Endres, M.W. Rutland, R. Bennewitz, R. Atkin, Control of Nanoscale Friction on Gold in an Ionic Liquid by a Potential-Dependent Ionic Lubricant Layer, Phys. Rev. Lett. 109 (2012) 155502. http://link.aps.org/doi/10.1103/PhysRevLett.109.155502.

- [12] Z. Li, F. Mangolini, Recent Advances in Nanotribology of Ionic Liquids, Exp. Mech. (2021). https://doi.org/10.1007/s11340-021-00732-7.
- [13] Z. Li, A. Dolocan, O. Morales-Collazo, J.T. Sadowski, H. Celio, R. Chrostowski, J.F. Brennecke, F. Mangolini, Lubrication Mechanism of Phosphonium Phosphate Ionic Liquid in Nanoscale Single-Asperity Sliding Contacts, Adv. Mater. Interfaces. 7 (2020) 2000426. https://doi.org/10.1002/admi.202000426.
- [14] B. Yu, D.G. Bansal, J. Qu, X. Sun, H. Luo, S. Dai, P.J. Blau, B.G. Bunting, G. Mordukhovich, D.J. Smolenski, Oil-miscible and non-corrosive phosphonium-based ionic liquids as candidate lubricant additives, Wear. 289 (2012) 58–64. https://doi.org/http://dx.doi.org/10.1016/j.wear.2012.04.015.
- [15] J. Qu, D.G. Bansal, B. Yu, J.Y. Howe, H. Luo, S. Dai, H. Li, P.J. Blau, B.G. Bunting, G. Mordukhovich, D.J. Smolenski, Antiwear Performance and Mechanism of an Oil-Miscible Ionic Liquid as a Lubricant Additive, ACS Appl. Mater. Interfaces. 4 (2012) 997–1002. https://doi.org/10.1021/am201646k.
- [16] J. Qu, H. Luo, M. Chi, C. Ma, P.J. Blau, S. Dai, M.B. Viola, Comparison of an oil-miscible ionic liquid and ZDDP as a lubricant anti-wear additive, Tribol. Int. 71 (2014) 88–97. https://doi.org/10.1016/j.triboint.2013.11.010.
- [17] W. Guo, Y. Zhou, X. Sang, D.N. Leonard, J. Qu, J.D. Poplawsky, Atom Probe Tomography Unveils Formation Mechanisms of Wear-Protective Tribofilms by ZDDP, Ionic Liquid, and Their Combination, ACS Appl Mater Interfaces. 9 (2017) 23152–23163. https://doi.org/10.1021/acsami.7b04719.
- [18] J. Qu, W.C. Barnhill, H. Luo, H.M. Meyer, D.N. Leonard, A.K. Landauer, B. Kheireddin, H. Gao, B.L. Papke, S. Dai, Synergistic Effects between Phosphonium-Alkylphosphate Ionic Liquids and Zinc Dialkyldithiophosphate (ZDDP) as Lubricant Additives, Adv. Mater. 27 (2015) 4767–4774. https://doi.org/10.1002/adma.201502037.
- [19] M. Han, R.M. Espinosa-marzal, Molecular Mechanisms Underlying Lubrication by Ionic Liquids: Activated Slip and Flow, (2018) 16–17. https://doi.org/10.20944/preprints201807.0248.v3.
- [20] M. Han, R.M. Espinosa-Marzal, Influence of Water on Structure, Dynamics, and Electrostatics of Hydrophilic and Hydrophobic Ionic Liquids in Charged and Hydrophilic Confinement between Mica Surfaces, ACS Appl. Mater. Interfaces. 11 (2019) 33465—

- 33477. https://doi.org/10.1021/acsami.9b10923.
- [21] Z. Wang, H. Li, R. Atkin, C. Priest, Influence of Water on the Interfacial Nanostructure and Wetting of [Rmim][NTf2] Ionic Liquids at Mica Surfaces, Langmuir. 32 (2016) 8818–8825. https://doi.org/10.1021/acs.langmuir.6b01790.
- [22] P. Wasserscheid, T. Welton, Ionic Liquids in Synthesis, 2nd ed., Wiley-VCH Verlag GmbH & Co. KGaA, 2003.
- [23] M.G. Freire, C.M.S.S. Neves, I.M. Marrucho, J.A.P. Coutinho, A.M. Fernandes, Hydrolysis of tetrafluoroborate and hexafluorophosphate counter ions in imidazolium-based ionic liquids, J. Phys. Chem. A. 114 (2010) 3744–3749. https://doi.org/10.1021/jp903292n.
- [24] M. Petkovic, K.R. Seddon, L.P.N. Rebelo, C.S. Pereira, Ionic liquids: A pathway to environmental acceptability, Chem. Soc. Rev. 40 (2011) 1383–1403. https://doi.org/10.1039/c004968a.
- [25] F. Mangolini, A. Rossi, N.D. Spencer, Chemical Reactivity of Triphenyl Phosphorothionate (TPPT) with Iron: An ATR/FT-IR and XPS Investigation, J. Phys. Chem. C. 115 (2011) 1339–1354. https://doi.org/10.1021/jp107617d.
- [26] C.J. Powell, The Physica B&Cl Basis for Quantitative Surface Analysis by Auger Electron Spectroscopy and X-Ray Photoelectron Spectroscopy, in: Quant. Surf. Anal. Mater. A Symp., 1978: pp. 5–30.
- [27] S. Tanuma, Electron Attenuation Lengths, in: D. Briggs, J.T. Grant (Eds.), Surf. Anal. by Auger X-Ray Photoelectron Spectrosc., Chichester: IM Publications, 2003: pp. 259–294.
- [28] G.H. Smudde, W.I. Bailey, B.S. Felker, M.A. George, J.G. Langan, Materials selection for HBr service, Corros. Sci. 37 (1995) 1931–1946. https://doi.org/10.1016/0010-938X(95)00075-U.
- [29] P.A. Byrne, Y. Ortin, D.G. Gilheany, First ever observation of the intermediate of phosphonium salt and ylide hydrolysis: P-hydroxytetraorganophosphorane, Chem. Commun. 51 (2015) 1147–1150. https://doi.org/10.1039/c4cc08644a.
- [30] B.J.J. Brophy, M.J. Gallagher, Phosphonium salts. I. The alkaline hydrolysis of some bisphosphonium salts, Aust. J. Chem. 22 (1969) 1385–98.
- [31] P.A. Byrne, D.G. Gilheany, The Mechanism of Phosphonium Ylide Alcoholysis and Hydrolysis: Concerted Addition of the O–H Bond Across the P=C Bond, Chem. A Eur.

- J. 22 (2016) 9140–9154. https://doi.org/10.1002/chem.201600530.
- [32] P. Haake, G.W. Allen, Alkaline hydrolysis of phosphine oxides in homogeneous solution. The nature of the pentacoordinate phosphorus intermediate, Tetrahedron Lett. 11 (1970) 3113–3116. https://doi.org/10.1016/S0040-4039(01)98428-X.
- [33] F. Gao, O. Furlong, P. V. Kotvis, W.T. Tysoe, Tribological properties of films formed by the reaction of carbon tetrachloride with iron, Tribol. Lett. 20 (2005) 171–176. https://doi.org/10.1007/s11249-005-8313-z.
- [34] F. Gao, P. V. Kotvis, W.T. Tysoe, The frictional behavior of thin halide films on iron, Tribol. Trans. 47 (2004) 208–217. https://doi.org/10.1080/05698190490431894.